題名　ISWI Newsletter - Vol. 3 No. 52
差出人　maeda@serc.kyushu-u.ac.jp

****
* ISWI Newsletter - Vol. 3 No. 52 16 May 2011 *
*
* I S W I = International Space Weather Initiative *
* (www.iswi-secretariat.org) *
*
* Publisher: Professor K. Yumoto, SERC, Kyushu University, Japan *
* Editor-in-Chief: Mr. George Maeda, SERC (maeda[at]serc.kyushu-u.ac.jp)*
* Archive location: www.iswi-secretariat.org (maintained by Bulgaria) *
* [click on "Publication" tab, then on "Newsletter Archive"] *
* Caveat: Under the Ground Rules of ISWI, if you use any material from *
* the ISWI Newsletter or Website, however minor it may seem *
* to you, you must give proper credit to the original source. *
****

Attachment(s):
(1) "Vecchio_2010", 503 KB pdf, 5 pages.
(2) "Vecchio_Carbone", 2.2 MB pdf, 7 pages.

: Re:
: Solar cyclic activity;
: Which ISWI array can check it?
:

Dear ISWI Participant:

I pass along this question to you from Dr Hans Haubold of UNOOSA:

"Which ISWI instrument array can provide data (for time series analysis)
to check solar cyclic activity as dealt with in the two attached papers? ".

I will print any comments received.

Sincerely,
: George Maeda
: The Editor
: ISWI Newsletter

The Astrophysical Journal Letters, 709:L1–L5, 2010 January 20 doi:10.1088/2041-8205/709/1/L1

QUASI-BIENNIAL MODULATION OF SOLAR NEUTRINO FLUX AND SOLAR AND GALACTIC COSMIC RAYS BY SOLAR CYCLIC ACTIVITY

A. Vecchio[1], M. Laurenza[2], V. Carbone[1,3], and M. Storini[2]
[1] Dipartimento di Fisica, Università della Calabria, 87036 Rende (CS), Italy; vecchio@fis.unical.it
[2] INAF/IFSI-Roma, 00133 Roma, Italy
[3] Liquid Crystal Laboratory (INFM), 87036 Rende (CS), Italy
Received 2009 September 11; accepted 2009 November 30; published 2009 December 29

ABSTRACT

Using some solar activity indicators such as sunspot areas and green-line coronal emission during the period 1974–2001, we find that the quasi-biennial periodicity is a fundamental mode of solar variability. We provide evidence for the quasi-biennial modulation of the solar neutrino flux, thus supporting the hypothesis of a connection between solar neutrinos and solar magnetic fields, probably through direct interaction with the neutrino magnetic moment. The same periodic modulation has been detected when fluxes of solar energetic protons and galactic cosmic rays are investigated. These modulation results significantly correlate to that of the neutrino flux. Finally, the superposition of the quasi-biennial cycle to the eleven-year cycle can explain the Gnevyshev Gap phenomenon.

Key words: methods: data analysis – neutrinos – Sun: activity – Sun: particle emission

Online-only material: color figures

One of the most interesting aspects of solar physics is the cyclic behavior of magnetic activity driven by the dynamo action, usually related to the emergence of a magnetic field in active regions. Apart from the eleven-year cycle, the most prominently recognized periods are the so-called quasi-biennial oscillations (QBOs) on timescales from 1.5 yr to 3.5 yr (Rao 1973; Rieger et al. 1984; Pap et al. 1990; Bay 2003; Knaack & Stenflo 2005; Vecchio & Carbone 2008, 2009; Valdés-Galicia & Velasco 2008). This periodicity is better detected in correspondence with cycle maxima and it suffers, as the eleven-year cycle does, from period length modulation (Vecchio & Carbone 2009). Quite interestingly, corresponding QBOs also have been found in other contexts related to solar variability, such as in solar wind fluctuations, interplanetary magnetic field intensity, galactic cosmic ray (CR) flux (e.g., Valdés-Galicia et al. 1996; Kudela et al. 2002; Mursula 2004), and, more recently, in the energetic proton fluxes recorded in interplanetary space (Laurenza et al. 2009) and in the solar rotation rate (Javaraiah et al. 2009). In an early attempt to solve the puzzle of missing neutrinos (Davis & Evans 1973), the existence of a quasi-biennial modulation for solar neutrinos has been claimed (Sakurai 1979; Haubold 1998; Shirai 2004; Sakurai et al. 2008; Sturrock 2009). To date the puzzle seems to be solved in favor of neutrino flavor transformation (Massetti & Storini 1996; Fukuda 1998), thus implying a rest mass for neutrinos. Nevertheless, the origin of the QBOs and their interaction with the solar magnetic field are still debated (Bahcall & Press 1991; Oakley et al. 1994; Krauss 1991; McNutt 1995; Wilson 2000; Sturrock 2008). Modulations of neutrino flux could come either from: (1) modulations of the neutrino's production rate by some yet unknown processes taking place inside the core of the Sun, or (2) coupling with the solar magnetic field. The latter hypothesis, if verified, would represent a confirmation of the existence of a magnetic moment for the neutrino, theoretically guaranteed by the detected neutrino's mass. Hence, the study of short-term periodicities of the solar cycle should lead to improved knowledge of the global properties of the Sun, with particular regard to solar neutrinos and energetic particle emission.

In the present Letter, we address the topic of the existence of the quasi-biennial solar cycle and its implications by investigating the time evolution of different data sets: the Fe XV 530.3 nm coronal green line (GL) brightness and sunspot areas (SA), along with the flux of the interplanetary protons in the energy range 0.50–0.96 MeV/nucleon, measured by the Charged Particles Measurements Experiment (channel P2) aboard the *IMP 8* spacecraft and the intensity of particles measured by the Rome Neutron Monitor (NM) with a cut-off rigidity of about 6 GV.[4] Finally we use two neutrino flux data sets, one from Homestake (ν) (a total of 108 records from 1974 to 1994; R. Davis 1994, private communication) and from super-Kamiokande (ν_K) experiments (a total of 184 records from 1996 to 2001; Fukuda 2001). The P2 data are largely representative of the low-energy solar CR flux, as the galactic contribution at energies lower than 1 MeV is practically negligible. On the other hand, NM data well represent the galactic CR flux (as the ground-level enhancements have been removed), which is modulated by the solar activity. All data sets, excluding neutrino fluxes, are monthly averaged and span 27 years from 1974 to 2001. Time evolution of the various data sets is reported in Figure 1. As a first step, we tried to identify the QBOs from the data sets through the Empirical Mode Decomposition (EMD), a technique developed to process non-stationary data (Huang et al. 1998) and successfully applied in many different contexts (Cummings et al. 2004). In the EMD framework, a time series $X(t)$ is decomposed into a finite number m of oscillating Intrinsic Mode Functions (IMFs) as

$$X(t) = \sum_{j=0}^{m-1} C_j(t) + r_m(t). \quad (1)$$

The IMFs $C_j(t)$ are a set of basis functions not assigned a priori, but rather obtained from the data set under analysis by following the procedure described by Huang et al. (1998). They represent zero mean oscillations with a characteristic timescale $\Delta\tau_j$, say

[4] SA at http://solarscience.msfc.nasa.gov/greenwch.shtml; GL provided by Dr. J. Sýkora; *IMP 8* data at http://sdwww.jhuapl.edu/IMP/imp_cpme_data.html; NM at http://www.fis.uniroma3.it/svirco/.

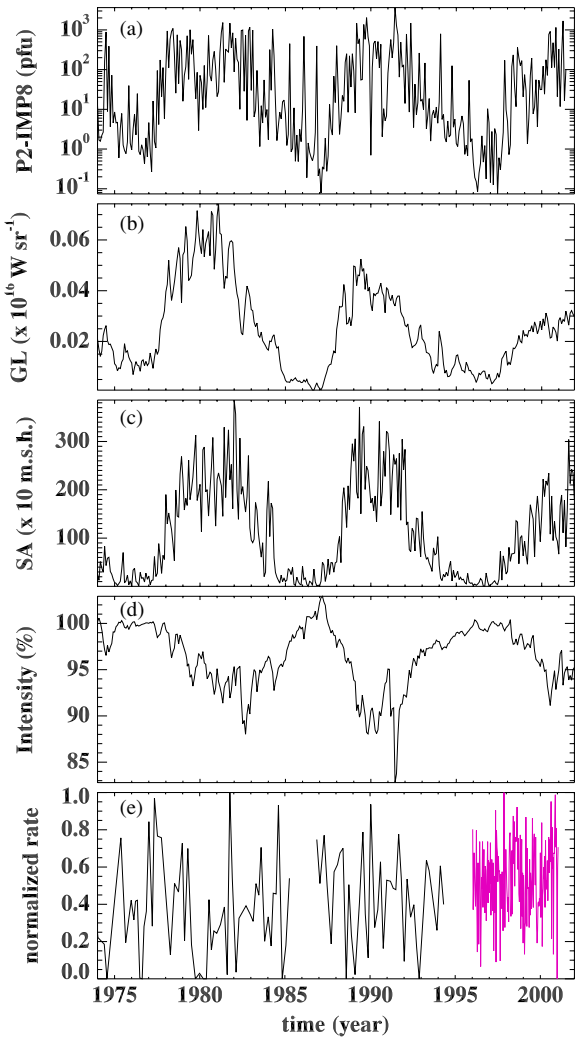

Figure 1. Time history of the P2 proton flux (a), the Fe XIV 530.3 nm coronal green line brightness (b), sunspot area (c), intensity of particles from the Rome neutron monitor (d), and neutrino fluxes (e) from Homestake (black line) and Super-Kamiokande (purple line) experiments.

(A color version of this figure is available in the online journal.)

the average spacing between extrema of the data. The IMFs are not restricted to a particular frequency but can experience both amplitude and frequency modulation. The residue $r_m(t)$ in Equation (1) describes the mean trend. This kind of decomposition is local, complete, and orthogonal; the orthogonality can be exploited to reconstruct the signal through partial sums in Equation (1) (Huang et al. 1998; Cummings et al. 2004; McDonald et al. 2007; Terradas et al. 2004). The statistical significance of information content for the IMFs with respect to a white noise can be checked by applying the test by Wu & Huang (1996) based on the following argument. When EMD is applied to a white noise series, the constancy of the product between the energy density of each IMF and its corresponding averaged period can be deduced. This relation can be used to derive the analytical energy density spread function of each IMF as a function of different confidence levels. Thus, by comparing the energy density of the IMFs extracted from the actual data with the theoretical spread function, one can distinguish IMFs containing information at the selected confidence level from purely noisy IMFs. By applying EMD to our data sets, we found one IMF oscillating at $\Delta\tau_j \simeq 11$ yr, which defines the basic solar cycle mode. In addition, IMFs, oscillating with timescales in the range 1.4 yr $\leqslant \Delta\tau_j \leqslant 4$ yr, are obtained for each data set. They are used to reconstruct the QBOs through partial sums in Equation (1). Their amplitudes are all above the 90% confidence level with respect to a white noise, with the exception of super-Kamiokande modes for which the confidence level is 75%. Further IMFs can be associated with other solar cycle periodicities, secular variations and noise. In particular, while QBOs and the eleven-year period are common to all data sets, particle time series (P2, NM, and ν) also show a significant typical timescale of about 7 yr. In Table 1, we report the information about the obtained EMD modes. The C_6 mode for NM data has an opposite phase with respect to GL, SA, and P2, which represents the well-known anti-correlation of CRs with respect to the eleven-year cycle of solar activity. The C_5 mode for ν flux has an average period of about $\Delta\tau_5 \simeq 13$ yr, which perhaps could be classified within the period–length modulation of the eleven-year cycle (Vecchio & Carbone 2009), although it is noticeably out of phase with all other eleven-year modes. In the present Letter we focus on QBOs, while a detailed analysis of the complete set of EMD modes will be reported in a future work. Time evolution of both QBOs and the eleven-year cycle for P2, GL, and SA data is reported in panels (a) and (b) of Figure 2, respectively. It is worthwhile to mention that our analysis about QBOs allows new information on the generation of the so-called Gnevyshev Gap (GG), defined as the time interval, during the maximum activity phase of each eleven-year cycle, in which a decrease in solar activity is observed; namely, the cycles have structured maxima, generally with a first peak at the end of the increasing phase and a second one at the start of the declining phase (see for a review Storini et al. (2003) and references therein). From panel (c) of Figure 2, we demonstrate that the superposition of the QBOs and the eleven-year cycle produces the GG feature, as conjectured in the past (Benevolenskaya 1998; Bazilevskaya et al. 2000). We also confirm that the amplitudes (see Figure 2 panel (a) and Figure 3) of the QBOs are enhanced around the years of maximum solar activity (Bazilevskaya et al. 2000; Mursula & Zieger 2000; Valdés-Galicia & Velasco 2008).

After identifying the QBO components through the EMD from the different indicators, they are compared by means of correlative analyses. As expected, the strongest values of correlation are found around the solar cycle maxima where the QBO amplitudes are higher. In particular, in Table 2 we report the Pearson correlation coefficients $r_{X,Y}$ between QBO signals for couples of parameters X and Y, obtained for a time interval lasting 1.5 yr around the times $T_{21} = 1980.25$ and $T_{22} = 1990.75$ for cycle 21 and cycle 22, respectively. Note that T_{21} and T_{22} correspond to the GG times derived from the P2 time series, for which the GG is more clearly apparent. When dealing with correlation between EMD modes, the Pearson coefficient is commonly used (Cummings et al. 2004). Nevertheless, there is no standard method for determining the significance of cross-correlations between single EMD modes or signals obtained through partial sums. In order to estimate the significance of the correlation coefficients, three independent statistical tests have been performed based on Fisher's transformation, bootstrap, and random phases approaches. Results are shown in Table 2, where Δr_F represents the 95% Fisher's confidence interval for the correlation coefficient. In the bootstrap analysis, Pearson's correlation coefficient r has been calculated for 10,000 different realizations of x- and y-parameters obtained through a resample of the original time series by picking an arbitrary set of subsamples (having the same number of data points) with replacements (i.e., an element may appear multiple times in a given bootstrap sample). By building the r histogram, the

Table 1
Information About the Obtained EMD Modes

Parameter	m	Eleven-year IMF	QBO IMFs	QBO Periods (yr)
GL	7	C_5	$C_3 + C_4$	$\tau_3 = 1.5 \pm 0.1$; $\tau_4 = 3.4 \pm 0.2$
SA	8	C_6	$C_4 + C_5$	$\tau_4 = 2.4 \pm 0.1$; $\tau_5 = 3.7 \pm 0.2$
P2	9	C_7	$C_4 + C_5$	$\tau_4 = 1.7 \pm 0.1$; $\tau_5 = 2.9 \pm 0.2$
NM	8	C_6	$C_3 + C_4$	$\tau_3 = 1.4 \pm 0.1$; $\tau_4 = 2.3 \pm 0.3$
ν	6	C_5 (?)	$C_2 + C_3$	$\tau_2 = 1.9 \pm 0.1$; $\tau_3 = 2.2 \pm 0.2$
ν_K	7	...	$C_5 + C_6$	$\tau_5 = 1.6 \pm 0.1$; $\tau_6 = 2.5 \pm 0.1$

Notes. Number (m) of EMD modes in Equation (1) for each data set; significant modes for the eleven-year cycle and QBOs along with their typical periods, calculated as the average time difference between local extrema. The standard error is provided for each period.

Table 2
Results of Correlative Analysis

	Cycle 21				Cycle 22			
X–Y	$r_{X,Y}$	Δr_F	$\Delta r_{\rm boot}$	$P_{\rm rp}$	$r_{X,Y}$	Δr_F	$\Delta r_{\rm boot}$	$P_{\rm rp}$
GL–SA	−0.47	[−0.76, −0.02]	[−0.76, 0.05]	0.30	0.98	[0.95, 0.99]	[0.97, 0.99]	0.01
P2–SA	0.18	[0.06, 0.59]	[−0.35, 0.60]	0.42	0.50	[0.06, 0.78]	[0.02, 0.77]	0.28
P2–GL	−0.73	[−0.89, −0.41]	[−0.92, −0.24]	0.14	0.60	[0.20, 0.83]	[0.10, 0.83]	0.20
P2–NM	−0.98	[−0.99, −0.95]	[−0.99, −0.97]	0.01	−0.92	[−0.97, −0.80]	[−0.96, −0.85]	0.03
SA–ν	0.10	[0.04, 0.53]	[−0.55, 0.57]	0.47	0.17	[0.07, 0.58]	[−0.31, 0.58]	0.43
GL–ν	−0.77	[−0.91, −0.49]	[−0.97, −0.23]	0.14	0.30	[0.18, 0.66]	[−0.20, 0.70]	0.37
P2–ν	0.96	[0.90, 0.98]	[0.91, 0.98]	0.01	0.93	[0.82, 0.97]	[0.82, 0.97]	0.03
NM–ν	−0.90	[−0.96, −0.75]	[−0.95, −0.78]	0.06	−0.99	[−0.99, −0.97]	[−0.99, −0.98]	0.01

Notes. Pearson correlation coefficients $r_{X,Y}$ between the QBOs of different couples of parameters X and Y during the maximum phases of cycles 21 and 22. Δr_F and $\Delta r_{\rm boot}$ represent the 95% confidence intervals for the correlation coefficient from Fisher's and bootstrap tests, respectively. $P_{\rm rp}$ indicates the probability, calculated through the random phases test, to obtain correlation values greater than $r_{X,Y}$ due to chance.

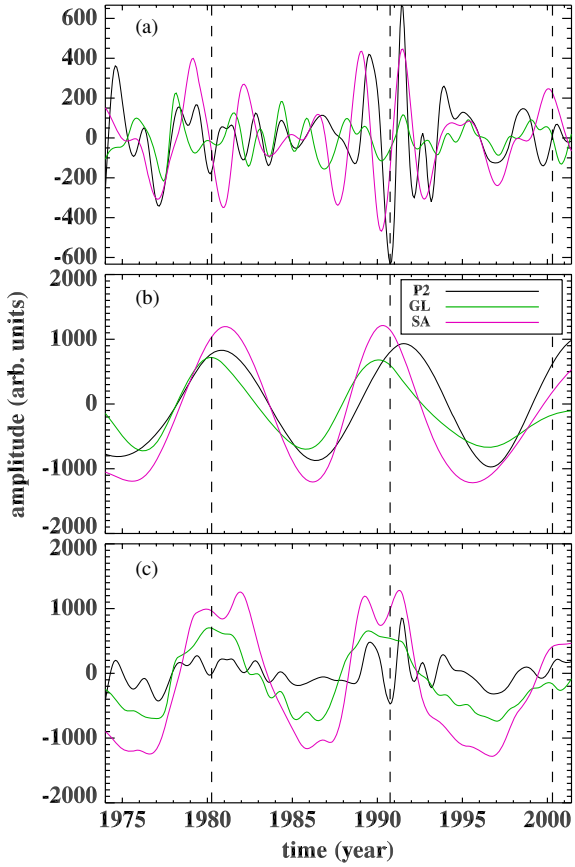

Figure 2. EMD reconstruction of both (a) QBOs and (b) eleven-year cycle for P2, GL, and SA, and (c) superposition of QBOs and eleven-year. Dashed lines indicate the time around which correlations are calculated.
(A color version of this figure is available in the online journal.)

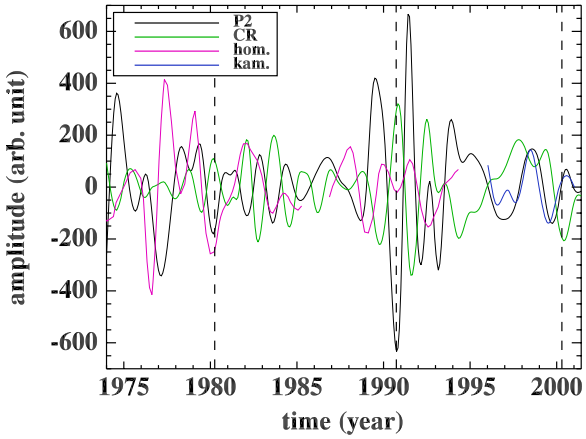

Figure 3. QBO reconstructed through the EMD for P2, NM, and neutrino fluxes. Dashed lines indicate the time around which correlations are calculated.
(A color version of this figure is available in the online journal.)

95% confidence interval $\Delta r_{\rm boot}$ for the correlation coefficient can be estimated. Finally, the random phases method (Simpson et al. 2001) allows one to compute the r histogram from 10,000 realizations of x, y obtained by randomizing the phases and keeping the amplitudes unchanged. The significance of Pearson's coefficient $r_{X,Y}$ can be estimated by summing up the values for $r > r_{X,Y}$ thus indicating the probability $P_{\rm rp}$ to obtain r values greater than $r_{X,Y}$ by chance.

While the eleven-year components are not perfectly in phase in both cycles (Figure 2(b)), a striking result is that QBOs for P2, GL, and SA are significantly correlated in cycle 22, while they are out of phase in cycle 21. It follows that the GG is almost synchronous and well shaped in cycle 22 for all the considered parameters, which is consistent with previous

findings (Bazilevskaya et al. 2000). We have to consider that the sunspot area is a proxy strictly related to the emergence of active regions on the solar photosphere whereas the GL brightness is more sensitive to changes in the configuration of the global magnetic field and the emission of solar CRs involves shock formation in the solar corona (e.g., Reames et al. 1999) or post-Coronal Mass Ejection reconnection processes (Cane et al. 1999; Klein & Posner 2005). Hence, the QBO behavior in cycle 21 results in non-synchronous multi-peaked or rather shallow two-peaked solar maxima observed for many parameters (Storini & Pase 1995; Feminella & Storini 1997; Storini et al. 2003; Bazilevskaya et al. 2000). In particular, we find that GGs in the P2 flux and SA are shifted in time similarly to the yearly number of SEP events and SA in cycle 21 (Bazilevskaya et al. 2006). This should be interpreted as the result of gross changes in the topology of the interplanetary magnetic field (van Allen 1988) and/or the incidence and intensity of magnetic discontinuities, which were associated with the reversal of polarity of the Sun's polar magnetic field during 1979–1981 (Rodríguez-Pacheco et al. 1997).

In order to clarify the last topic, we analyzed the variability of the galactic CR intensity, which are strongly influenced by the variations of the global magnetic field of the Sun. The QBOs have been clearly detected through the EMD technique in the NM data, as displayed in Figure 3. A significant anti-correlation $r_{P2,\mathrm{NM}} = -0.59$ between the QBOs of P2 and NM is obtained throughout the whole period 1974–2001. The correlation is even stronger during the maximum phases (see Table 2). An anti-correlation between solar and galactic CRs, although well known for the eleven-year component, has never been detected in this range of frequency. This strong anti-correlation represents an indirect confirmation of the existence of the quasi-biennial cycle in the evolution of the solar magnetic field, which affects the two CR populations in opposite ways.

A surprising result comes from the clear observation of QBOs also for neutrino fluxes (cf. Figure 3). While the existence of quasi-biennial modulation in solar neutrino flux has been claimed from several experiments (Sakurai et al. 2008) its correlation with the solar activity has never been absolutely proved. We remark that, since the solar indicator signals are dominated by the eleven-year period of the main cycle, QBOs in rough data cannot be directly correlated with those eventually present in neutrino fluxes, but usually running means or smoothing procedures are applied (Massetti & Storini 1996; Boyer et al. 2000). Moreover, it has been claimed that when an indicator exhibits the eleven-year periodicity, no reliable values of correlations could be obtained (Walther 1997). On the contrary, in the present Letter, the EMD is used as a filter to isolate (by partial sums of single IMFs) the QBOs contribution from the rough time series and their correlation is directly calculated without averages or smoothing.

We find a strong positive (negative) correlation between the QBO of the Homestake neutrino flux and the corresponding P2 (NM) mode, mainly evident at the solar maxima. According to the performed tests, the correlations are significant (Table 1). This indicates that a strong magnetic field is perhaps necessary to affect the neutrino flux. No correlations between neutrino flux and SA and GL are found. By considering also the QBO relative to the super-Kamiokande data set (Figure 3), we observe a strong correlation between ν_K and both P2 and NM fluxes, namely $r_{\nu_K,P2} = 0.94$ ($\Delta r_F = [0.85, 0.98]$, $\Delta r_{\mathrm{boot}} = [0.89, 0.97]$ and $P_{\mathrm{rp}} = 0.006$) and $r_{\nu_K,NM} = -0.92$ ($\Delta r_F = [-0.97, -0.80]$, $\Delta r_{\mathrm{boot}} = [-0.97, -0.78]$ and $P_{\mathrm{rp}} = 0.01$), respectively, during a period lasting 1.5 yr around the time $T_{23} = 2000.3$, say the time of cycle 23 maximum as indicated on the NOAA Web site.

As a conclusion, the QBOs are a fundamental mode of solar activity that greatly affect the fluxes of both solar and galactic CRs and neutrinos. In particular, our findings represent strong evidence of a relationship between solar neutrino flux and solar activity. Our approach is somewhat different from earlier attempts where the neutrino flux, dominated by QBOs, was directly compared with the eleven-year solar cycle described by SA or sunspot numbers, which cannot represent the complexity of the solar magnetic cycle. On the contrary, we compare the proper oscillating components of the solar cycle at the same time scale, selected through EMD. Since the modulations of both NM and P2 are driven by the solar magnetic field, the strong correlation found between neutrinos and the two populations of CRs suggests that the magnetic flux plays a crucial role in the modulation of the solar neutrino flux as well, probably involving magnetic moment interactions through the spin-flavor precession (Voloshin & Vysotskii 1986).

We thank the referee for useful comments. This work was partially supported by ASI/INAF contracts I/090/06/0 and I/015/07/0, by INAF (PRIN 2007) "Scientific exploitation of the Interferometric Bidimensional Spectrometer (IBIS) Magnetic structuring of the lower solar atmosphere." Thanks are due to PNRA for the use of the RAC-ANT database.

REFERENCES

Bahcall, J. N., & Press, W. H. 1991, ApJ, 370, 730
Bay, T. 2003, ApJ, 591, 406
Bazilevskaya, G. A., Krainev, M. B., Makhmutov, V. S., Flückiger, E. O., Sladkova, A. I., & Storini, M. 2000, Sol. Phys., 197, 157
Bazilevskaya, G. A., Makhmutov, V. S., & Sladkova, A. I. 2006, Adv. Space Res., 38, 484
Benevolenskaya, E. E. 1998, ApJ, 509, L49
Boyer, J., Hahn, R. L., & Cumming, J. B. 1986, ApJ, 537, 1080
Cane, H. V., Erickson, W. C., & Prestage, N. P. 2002, J. Geophys. Res., 107, 14
Cummings, D. A. T., et al. 2004, Nature, 427, 344
Davis, R., Jr., & Evans, J. C. 1973, Proc. 13th ICRC (Denver), 3, 2001
Feminella, F., & Storini, M. 1997, A&A, 322, 311
Fukuda, S., et al. 2001, Phys. Rev. Lett., 86, 5651
Fukuda, Y., et al. 1998, Phys. Rev. Lett., 81, 1562
Haubold, H. J. 1998, Ap&SS, 258, 201
Huang, N. E., et al. 1998, Proc R. Soc. Lond. A, 454, 903
Javaraiah, J., Ulrich, R. K., Bertello, L., & Boyden, J. E. 2009, Sol. Phys., 257, 61
Klein, K.-L., & Posner, A. 2005, A&A, 438, 1029
Knaack, R., & Stenflo, J. O. 2005, A&A, 438, 349
Krauss, L. M. 1991, Nature, 348, 403
Kudela, K., Rybak, J., Antalová, A., & Storini, M. 2002, Sol. Phys., 205, 165
Laurenza, M., Storini, M., Giangravé, S., & Moreno, G. 2009, J. Geophys. Res., 114, A01103
Massetti, S., & Storini, M. 1996, ApJ, 472, 827
McDonald, A. J., Baumgaertner, A. J. G., Fraser, G. J., George, S. E., & Marsh, S. 2007, Ann. Geophys., 25, 375
McNutt, R. L. 1995, Science, 270, 1635
Mursula, K., & Vilppola, J. H. 2004, Sol. Phys., 221, 337
Mursula, K., & Zieger, B. 2000, Adv. Space Res., 25, 1939
Oakley, D. S., Snodgrass, H. B., Ulrich, R. K., & Van De Kop, T. L. 1994, ApJ, 437, L63
Pap, J., Tobiska, W. K., & Bouwer, S. D. 1990, Sol. Phys., 129, 165
Rao, K. R. 1973, Sol. Phys., 29, 47
Reames, D. V., Ng, C. K., & Tylka, A. J. 1999, Geophys. Res. Lett., 26, 3585
Rieger, E., Kanbach, G., Reppin, C., Share, G. H., Forrest, D. J., & Chupp, E. L 1984, Nature, 312, 623
Rodríguez-Pacheco, J., Sequeiros, J., del Peral, L., Medina, J., & Wenzel, K.-P. 1997, J. Geophys. Res., 102, 9801
Sakurai, K. 1979, Nature, 278, 146

Sakurai, K., Haubold, H. J., & Shirai, T. 2008, Space Rad., 5, 207
Shirai, T. 2004, Sol. Phys., 222, 199
Simpson, D. M., Infantosi, A. F. C., & Botero Rosas, D. A. 2001, Med. Biol. Eng. Comput., 39, 428
Storini, M., Bazilevskaya, G. A., Fluckiger, E. O., Krainev, M. B., Makhmutov, V. S., & Sladkova, A. I. 2003, Adv. Space Res., 31, 895
Storini, M., & Pase, S. 1995, STEP GBRSC News, 5, 255 (special issue)
Sturrock, P. A. 2008, ApJ, 688, L53
Sturrock, P. A. 2009, Sol. Phys., 254, 227
Terradas, J., Oliver, R., & Ballester, J. L. 2004, ApJ, 614, 435
Valdés-Galicia, J. F., Perez-Enriquez, R., & Otaola, J. A. 1996, Sol. Phys., 167, 409
Valdés-Galicia, J. F., & Velasco, V. M. 2008, Adv. Space. Res., 41, 297
van Allen, J. A. 1988, Geophys. Res. Lett., 15, 1527
Vecchio, A., & Carbone, V. 2008, ApJ, 683, 536
Vecchio, A., & Carbone, V. 2009, A&A, 502, 981
Voloshin, M. B., & Vysotskii, M. I. 1986, Sov. J. Nucl. Phys., 44, 544
Walther, G. 1997, Phys. Rev. Lett., 79, 23
Wilson, R. M. 2000, ApJ, 545, 532
Wu, Z., & Huang, N. E. 2004, Proc. R. Soc. Lond. A, 460, 1597

A&A 502, 981–987 (2009)
DOI: 10.1051/0004-6361/200811024

Astronomy & Astrophysics

Spatio-temporal analysis of solar activity: main periodicities and period length variations

A. Vecchio[1] and V. Carbone[1,2]

[1] Dipartimento di Fisica, Universitá della Calabria, Ponte P. Bucci cubo 31C, 87036 Rende (CS), Italy
e-mail: vecchio@fis.unical.it
[2] Liquid Crystal Laboratory, INFM/CNR, Ponte P. Bucci cubo 33B, 87036 Rende (CS), Italy

Received 23 September 2008 / Accepted 8 May 2009

ABSTRACT

Aims. The spatio-temporal dynamics of solar activity has been investigated by studying the main oscillations and the time evolution of the basic periods.
Methods. The spatio-temporal behavior of the green coronal emission line at 530.3 nm, recorded from 1939 to 2005, has been analyzed by using proper orthogonal decomposition, to extract the main components of the system, and the wavelet analysis to further investigate their time behaviour.
Results. In addition to the main 11-year periodicity, a high-frequency component has been recorded mainly on the polar regions of the Sun, thus indicating a different origin from the emergence of active regions. Evidence for variations in the period lengths of this component has been found for the first time. The calculated period length varies between 1.5 years and 4 years, in good agreement with frequencies attributed to the quasi-biennial cycle extracted by different solar activity indicators. Our analysis shows that, unlike the main periodicity, the high-frequency component does not show the typical properties of a true mode of oscillation but seems to originate, in a narrow band of frequencies, from a stochastic superposition of different oscillators.
Conclusions. The observed solar cycle frequencies in the range 1.5–4 years, commonly considered as independent modes of oscillation, could be the manifestation of the temporal modulation of a unique quasi-biennial periodicity. Our findings can provide more constraints on dynamo models introduced to describe the different components of the solar cycle. The calculated period length variations could also be helpful to improve our knowledge of the relationship between solar activity, neutrino flux variations and cosmic ray modulation.

Key words. Sun: activity – methods: data analysis – Sun: corona

1. Introduction

It is well known that solar magnetic activity is characterized by a periodic behavior of about 11 years (cf. e.g. Stix 2002), usually related to the emergence of magnetic field at active regions within the photosphere. Although the most evident signature of the solar activity is the cyclic time variation of the sunspot number, the 11-year periodicity can be also recognized by looking at different indicators (e.g. flares occurrence, 10-cm flux, Ca K index). The length of this main cycle is not constant (Eddy 1976; Friis-Christensen & Lassen 1991; Fligge et al. 1999), rather, an apparently stochastic time modulation generates a kind of "solar melody" (Beer et al. 1994). This relates the solar activity to effects on the Earth's climate. In fact, even if the topic is under debate (see e.g. Scafetta & West 2008), it has been pointed out that a high correlation exists between the solar cycle length and the northern hemisphere Earth temperature records (Friis-Christensen & Lassen 1991).

Short-term periodicities in the solar activity range from few days to years (e.g. Gnevyshev 1977; Rušin & Zverko 1990; Bay 2003; Kane 2005; Vecchio et al. 2005; Penza et al. 2006). Among the yearly periodicities, the most noticeable periods are 1.3 years and 3.6 years, along with some periods in the range between 2.6 years and 2.8 years (for a complete classification of the high-frequency periodicities observed in many solar indices see e.g. Kane 2005). Many authors (Krivova & Solanki 2002; Knaack et al. 2004, 2005; Cadavid et al. 2005; Li et al. 2006), using different techniques of analysis and different activity indicators, have shown that the observed high frequency periodicities are not recognized as a typical feature of every solar cycle but seem to appear only from time to time. A corresponding quasi-biennial periodicity has also been found in contexts related to solar variability. The first evidence of this is the quasi-biennial oscillation of solar neutrino fluxes first observed by Sakurai (1979) with the Homestake experiment and followed by different detections from the GALLEX (GNO) and the Super-Kamiokande experiments (e.g. Haubold 1998; Shirai 2004; Sakurai et al. 2008). In another context, a quasi-biennial variation has been detected in the proton fluxes recorded by the CPME instrument, onboard IMP 8, in the interplanetary space in the energy bands $0.50 \div 0.96$ MeV and $190 \div 440$ MeV (Laurenza et al. 2009).

The study of short-term periods in the Sun and defining their properties can be very interesting since:

- they can provide useful information on the global properties of the Sun (Benevolenskaya 1998; Vecchio & Carbone 2008a,b), for example on the solar dynamo theory;
- the short-term periodicities can be related to the time variation of neutrino solar flux and proton fluxes in interplanetary space;
- in the case of non-constant period lengths they could enrich the "solar melody" with further components, perhaps

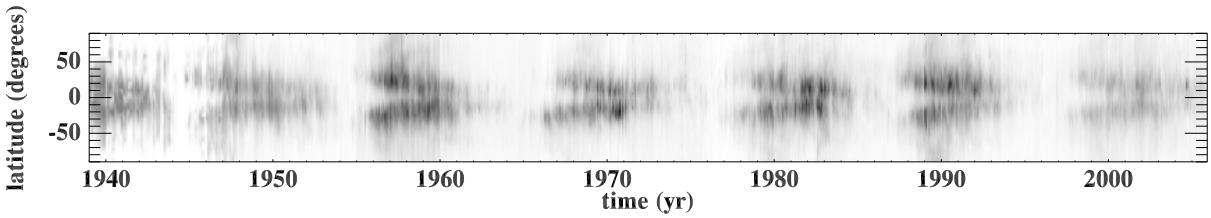

Fig. 1. The daily intensity emission of the solar corona in the period 1939–2005 as observed in the time-angle plane. The latitude $\theta = 0$ corresponds to solar equator. The color scale is linear.

influencing the climate on Earth (Friis-Christensen & Lassen 1991).

The present paper addresses these points by analyzing the spatio-temporal properties of solar activity and by searching for variations in the period length of the components of the solar cycle. We will show the results of a spatio-temporal analysis on the green coronal emission line at 530.3 nm by using proper orthogonal decomposition (POD) (Holmes 1996) together with the well known wavelet analysis. In particular, the first technique is able to identify and separate the contribution of the short-term components from the main solar cycle, while wavelets are useful to characterize the time behavior of the various POD modes. The period length variations can be calculated from the wavelet spectra by using a method developed by Fligge et al. (1999). By using the POD as a filter, we are able to identify the short-term signal more clearly than in the raw data. The POD analysis allows us to recognize that the main cycle and the quasi-biennial periodicity are generated by different phenomena in the framework of the dynamo effect. In particular, the short-term component is likely to be generated by a stochastic phenomenon, since the observed quasi-biennial cycle results from a superposition of different oscillators with random phases rather than a pure oscillating phenomenon.

2. Data analysis

The data set[1] consists of a scalar field $I(\theta, t)$ representing monthly observations (in the period 1939–2005) of the green coronal emission line Fe XIV at 530.3 nm. Each month, 72 values of intensities, in millionths of intensity of the solar disk, from $0 \le \theta \le 355$ degrees of latitude (in increments of 5 degrees) are given. The green coronal emission dynamics has been investigated in the past (Mininni 2002; Vecchio et al. 2005; Vecchio & Carbone 2008b) to characterize the solar activity. Here we analyze the revised data set of green coronal emission (Rybanský et al. 2005). This new data set has been corrected for an anomalous monotonic increase of the maximum of coronal emission from cycle 18 to cycle 20. With respect to the uncorrected coronal emission, the chosen set shows some advantages, namely:

- the amplitudes of the found solar cycle periodicities can be correctly quantified;
- these values of the coronal emission enable the exact time localization of the different short-term periodicities;
- the calculated period length variations are not affected by spurious contributions due to an artificial activity increase.

Figure 1 shows the spatio-temporal plot of the dataset. All features characterizing the solar cycle, namely the temporal 11-year period and the migration of activity toward the solar equator giving rise to the butterfly diagram, are visible.

In a first step, the spatio-temporal field $I(\theta, t)$ has been analyzed through POD. In this framework the coronal emission can be described by a superposition of N modes (Holmes 1996), characterized by temporal modal coefficients $a_j(t)$ and spatial basis functions $\Psi_j(\theta)$ not fixed a priori:

$$I(\theta, t) = \sum_{j=0}^{\infty} a_j(t)\Psi_j(\theta). \tag{1}$$

The basis functions in (1) are calculated by maximizing the averaged projection of $I(\theta, t)$ onto $\Psi_j(\theta)$ constrained to unitary norm, which leads to a Fredholm integral equation

$$\int_{L_\theta} \mathrm{d}\theta' \langle I(\theta, t) I^*(\theta', t)\rangle \Psi(\theta') = \lambda \Psi(\theta) \tag{2}$$

in which L_θ represents the lengths of spatial integration domain and brackets are time averages. The solution provides both eigenfunctions Ψ_j and eigenvalues λ_j, ordered such that $\lambda_j \ge \lambda_{j+1}$. λ_js are a countable set and represent the energy associated with each mode, quantifying the relative contribution of each mode to the signal reconstruction. The POD temporal coefficients are then calculated by projecting the original field onto the corresponding basis functions. A reconstruction of the field by selectively choosing a finite number N of the most energetic modes is possible. In this way, we form a subspace spanned by the first N eigenfunctions

$$I(\theta, t) = \sum_{j=0}^{N} a_j(t)\Psi_j(\theta). \tag{3}$$

The POD procedure yields a complete set of modes that are optimal in energy (Holmes 1996), thus a truncated POD expansion such as (3) describes typical members of the ensemble better than any other decomposition of the same truncation order. This analysis has been used in solar physics to investigate some different properties of the solar cycle (Mininni 2002; Vecchio et al. 2005; Vecchio & Carbone 2008b), photospheric turbulence (Vecchio et al. 2008) and magnetic field evolution (Rees 2000; Lawrence 2004).

3. Results

Excluding the number and area of sunspot, the coronal emission represents the longest solar activity indicator providing

[1] The full data set is available at `ftp://ftp.ngdc.noaa.gov/STP/SOLAR_DATA/SOLAR_CORONA/LOMNICKY/5-degree-data/`. The coronal intensities are given in millionths of intensity of the solar disk (coronal units) and converted to the photometrical scale of Lomnický Štít Station at a height of 40″ above the solar limb (cf. Rybanský 1994; Rybanský et al. 2005). Several stations were used in this database, namely: Lomnický Štít, Sacramento Peak, Norikura, Kislovodsk, Pic Du Midi, Wendelstein, Arosa, and Kanzelhöhe. Lomnický Štít is the primary station since 1965.

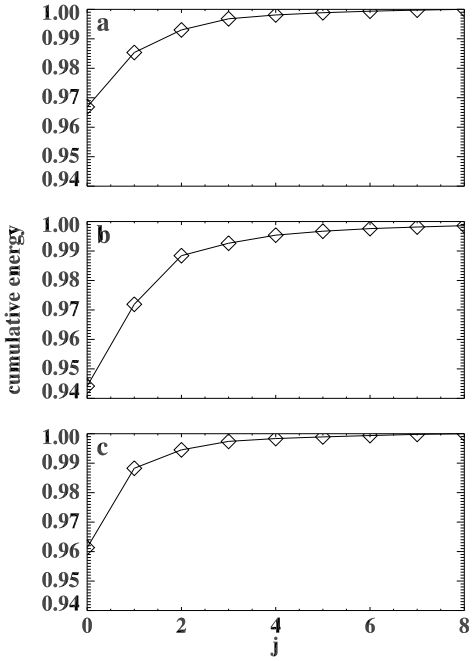

Fig. 2. Cumulated energy of the first nine POD modes as a function of the index j ($j = 0, \ldots, 8$). Panel **b)** refers to the equatorial sample, panels **a)**, **c)** correspond to polar data sets.

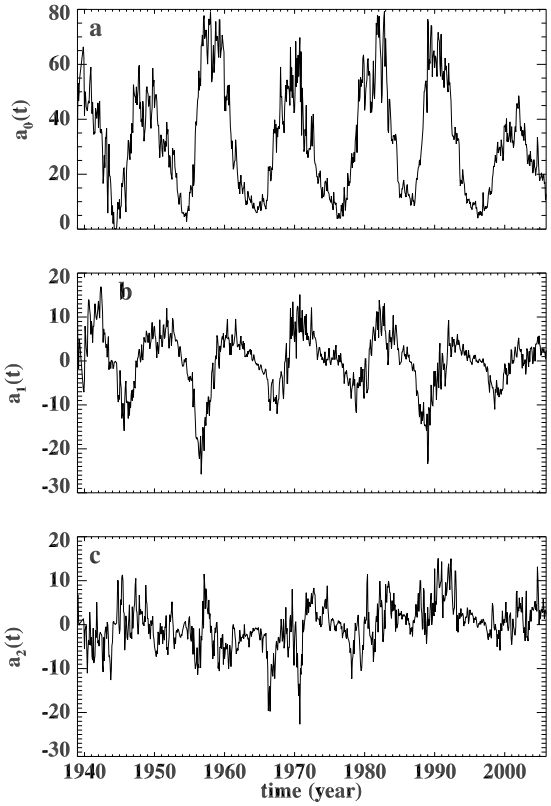

Fig. 3. *Equatorial data set*: time evolution of the first three POD coefficients $a_j(t)$ for $0 \le j \le 2$.

spatial information. However, while sunspot properties are related to the emergence of magnetic field in the active regions, $I(\theta, t)$ also contains information about the global solar magnetic field. The contribution of the active regions and large scale magnetic fields to the coronal emission can be coarsely separated by dividing the whole dataset into three main regions according to their latitudes: i) an equatorial region, in the latitude range $-45° \le \theta \le 45°$, associated with the active region emergence; ii) two polar areas, a northern and a southern region in the range of latitudes $50° \le \theta \le 90°$ and $-90° \le \theta \le -50°$ (from the equatorial plane) respectively.

3.1. Spatio-temporal characteristics of solar activity

The POD has been applied to each region separately, thus obtaining a set of coefficients $a_j(t)$ and eigenfunctions $\Psi_j(\theta)$ ($j = 0, \ldots, 18$ for equatorial region, and $j = 0, \ldots, 8$ for poles) which furnish information about the spatio-temporal dynamics of the solar cycle.

In Fig. 2 we report, for all samples, the cumulated energies of the first nine ($j = 0, \ldots, 8$) POD modes. About 99% of the total energy is shared among the first three modes $j = 0 \div 2$ for the equatorial sample (Fig. 2, panel b), and between the first two modes $j = 0 \div 1$ for the polar samples (Fig. 2, panels a, c). This means that the first few POD modes, together containing 99% of the energy, suffice to describe the main features of the solar cycle at both high and equatorial latitudes.

The POD analysis is a very efficient tool to recognize and to select individual contributions to the solar cycle, according to their spatial pattern, and their time behavior is directly described by the coefficients $a_j(t)$. The POD coefficients corresponding to the high energy modes for the equatorial and polar samples are shown in Figs. 3 and 5. In Fig. 3 (panels a,b) it can be seen that the first two most energetic modes ($j = 0, 1$) describe the main 11-year cycle. However, $a_0(t)$ and $a_1(t)$, although characterized by the same periodicity, can be associated with different feature of the global pattern since they are out of phase and are characterized by non-correlated amplitude fluctuation. This is clear by looking at the spatio-temporal intensities (Fig. 4, panels a,b), reconstructed according to Eq. (3). While the mode $j = 0$ is associated with the basic 11-year spatial periodicity, the mode $j = 1$ describes the north-south occurrence of the active region contributing to the butterfly wings in the usual time-latitude diagrams. The lower energy $j = 2$ mode, which seems to contain many spatial scales (see Fig. 3, panel c), describes small scale fluctuations of the main solar cycle. The effect of this mode on the spatio-temporal intensity pattern (Fig. 4, panel c) is to enhance the fluctuations of the signal and to form the north-south asymmetries in the wings of the butterfly diagram (see e.g. Pontieri et al. 2003; Knaack et al. 2004; Badalyan et al. 2008).

Conversely, only the $j = 0$ mode is associated with the main 11-year solar cycle in both polar regions (Fig. 5, panels a,b). At these latitudes, the main cycle does not show a complex spatial structure, thus one POD mode suffices to describe it. At first sight, $a_1(t)$ coefficients, from both north and south regions, show high frequency fluctuations but no evident oscillating behavior can be seen. These modes could thus represent a stochastic short-term component of the cycle. Reconstructions of the coronal emission at high latitude using only the first $j = 0, 1$ modes are shown in Fig. 6

The main spatio-temporal peculiarities of solar activity are explained within the context of dynamo theory. In this framework, the magnetic field of the Sun is generated through a turbulent $\alpha - \omega$ process. Our results provide observational constraints for theoretical modeling of the solar dynamo effect. Firstly, the nature of the 11-year and the high frequency contributions are quite different. This can be inferred by simply studying the time behaviour of the main polar and equatorial coefficients $a_j(t)$ by

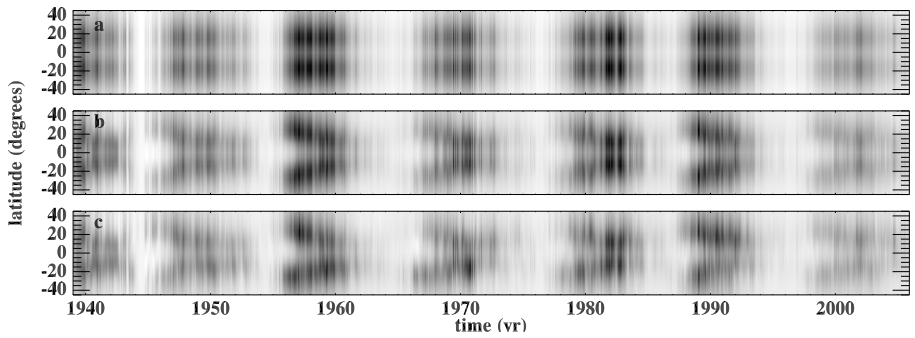

Fig. 4. Reconstructed intensity $I(\theta, t)$ for the equatorial area, represented in the (t, θ) plane, using different N in Eq. (3). $N = 0$ (panel **a)**), $N = 1$ (panel **b)**). $N = 2$ (panel **c)**) contains the 99% of the total energy. The color scale is linear.

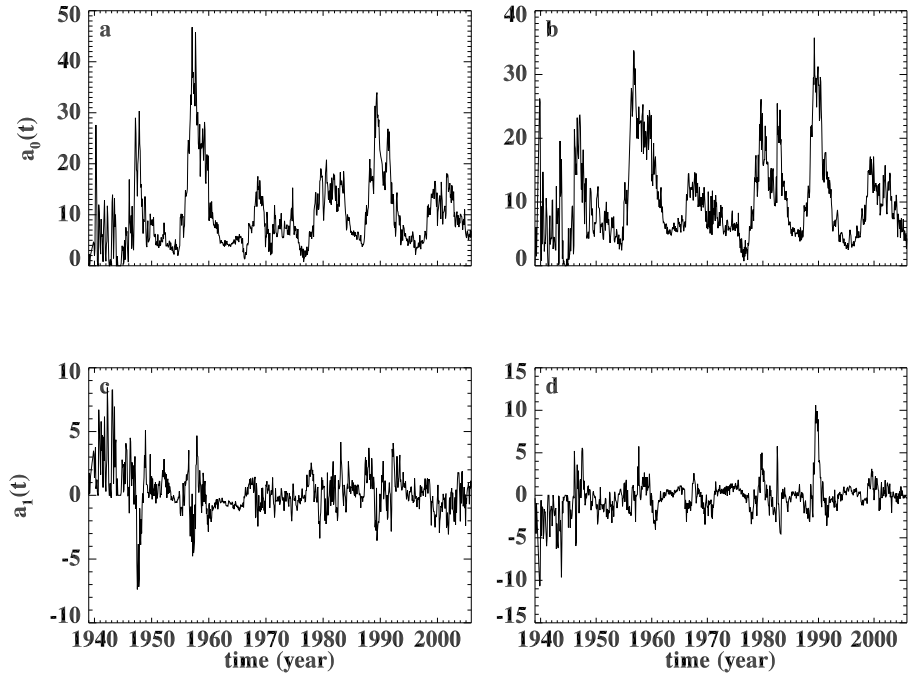

Fig. 5. *Polar data sets*: time evolution of the first two POD coefficients $a_j(t)$ for $j = 0, 1$ for the northern (panels **a)**, **c)**) and southern regions (panels **b)**, **d)**).

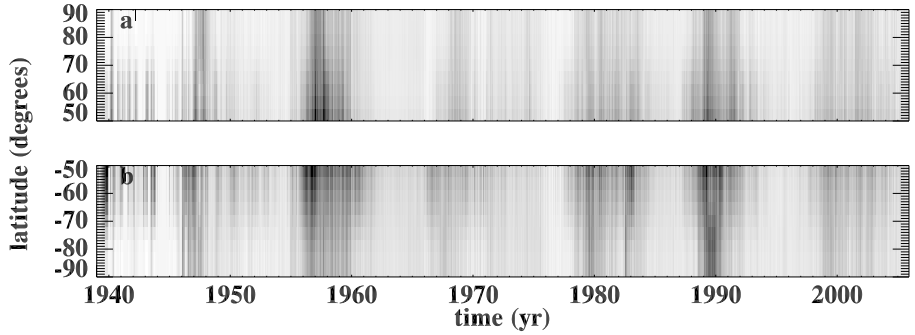

Fig. 6. Reconstructed intensity $I(\theta, t)$, using the first two modes containing 99% of the total energy, represented in the (t, θ) plane. Panel **a)** refers to the northern region and panel **b)** to the southern region.

building up a kind of phase space. This is defined by plotting two coefficients, one versus the other. Since the equatorial $a_0(t)$, $a_1(t)$ and the polar $a_0(t)$ describe the main solar cycle while both polar $a_1(t)$ are associated with the high-frequency components, we will study how the phase space is modified when the coefficients on the plot axis are changed. Figure 7 shows the phase space of the equatorial $a_1^{\rm eq}(t)$ versus the equatorial $a_0^{\rm eq}(t)$ (panel a), the polar $j = 0$ coefficients versus the equatorial $a_0^{\rm eq}(t)$ (panel b,c) and both polar $j = 0$ coefficients, namely $a_0^s(t)$ versus $a_0^n(t)$ (panel d). These coefficients are associated with the main solar periodicity, thus the phase space plots appear quite regular, excluding small local fluctuations of phase and frequency, and indicate that two orthogonal oscillators, with the same frequency, are present. More precisely, while panel a, characterized by more or less concentric and rotating ellipses, describes two out of phase oscillations with non-correlated amplitude variations, phase spaces b–d, in which the points are sorted approximately along a straight line, can be associated with oscillations with zero phase difference and correlated amplitude variations. The behaviour illustrated in panel a can be explained by remembering that equatorial $j = 0, 1$ modes describe different aspects of the solar activity, namely the basic spatial periodicity and the north-south occurrence of the active regions. Both phenomena show the same periodicity in time, but the amplitudes and phase difference change in a different way.

This is a clear indication that the main solar cycle represents a true oscillation mode and thus it can be described by a simple nonlinear oscillator (Mininni et al. 2000; Pontieri et al. 2003)

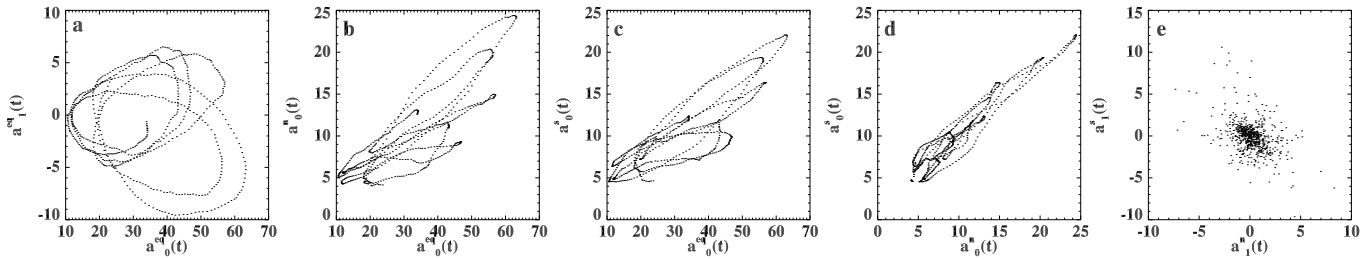

Fig. 7. Phase space of two POD coefficients. **a)**: $a_0^{eq}(t)$ versus $a_1^{eq}(t)$ for the equatorial data set. **b), c)**: equatorial $a_0^{eq}(t)$ versus northern and southern $a_0(t)$. **d)**: northern $a_0^n(t)$ versus southern $a_0^s(t)$. **e)**: northern $a_1^n(t)$ versus southern $a_1^s(t)$.

within a narrow band of frequencies and with a well defined phase.

The phase space of the $j = 1$ polar coefficients (panel e), associated with the short-term component of the solar activity, shows a stochastic behavior. This kind of plot is very different from the phase space generated by two coherent oscillations. These simple considerations indicate that the short term component of the solar activity is probably generated by a turbulence-like phenomenon in a narrow band of frequencies. Dynamo models describing the source of solar periodicities must take into account these properties.

3.2. Time evolution of POD coefficients: Wavelet analysis and period length variation

Wavelets have been chosen to study the temporal behaviour of the POD modes and to characterize the high frequency modulation of coefficients $a_j(t)$. To this purpose, the well known Mexican Hat Wavelet analysis (Torrence & Compo 1998) has been applied to each $a_j(t)$ thus obtaining a set of wavelet coefficients $W_j(T,t)$ (T is the period). The choosen form for the wavelet mother function ensures a good compromise between spatial and temporal resolution (Torrence & Compo 1998).

Figures 8 and 9 show the local wavelet power spectrum $|W_j(T,t)|^2$ in the time-period domain (left figure of each panel) and the global wavelet spectrum $P_j(T) = \int |W_j(T,t)|^2 dt$ (right figure of each panel) respectively for the equatorial and polar data sets. The local spectrum contains information on the time localization of the detected frequencies. The global spectra, being integrated over time, are analogous to the Fourier spectra and are helpful to detect the dominant frequencies at work in the system. When the frequencies are strongly modulated in time, global and local spectra could give different results. In fact the time integration, performed in the $P_j(T)$ calculation, produces strong peaks when the frequency is almost constant in time. In Figs. 8 and 9, cross-hatched regions represent the cone of influence (COI), namely the area of the local wavelet spectrum in which edge effects become important (Torrence & Compo 1998), thus influencing the result. The color scale, chosen to draw spectra, associates blue with low power and yellow with high power areas, passing through green and red. The significance levels for the spectra are established through statistical significance tests developed by deriving theoretical wavelet spectra for white noise processes (Torrence & Compo 1998).

Let us consider in detail Figs. 8 and 9. The local wavelet power is distributed along ridges around 11 years both for equatorial $j = 0, 1$ (Fig. 8, panels a, b) and polar $j = 0$ coefficients (Fig. 9, panels a, b). This is confirmed by a look at the global power spectrum, dominated by a peak at a period of about 11 years. The global wavelet spectra also reveal a power

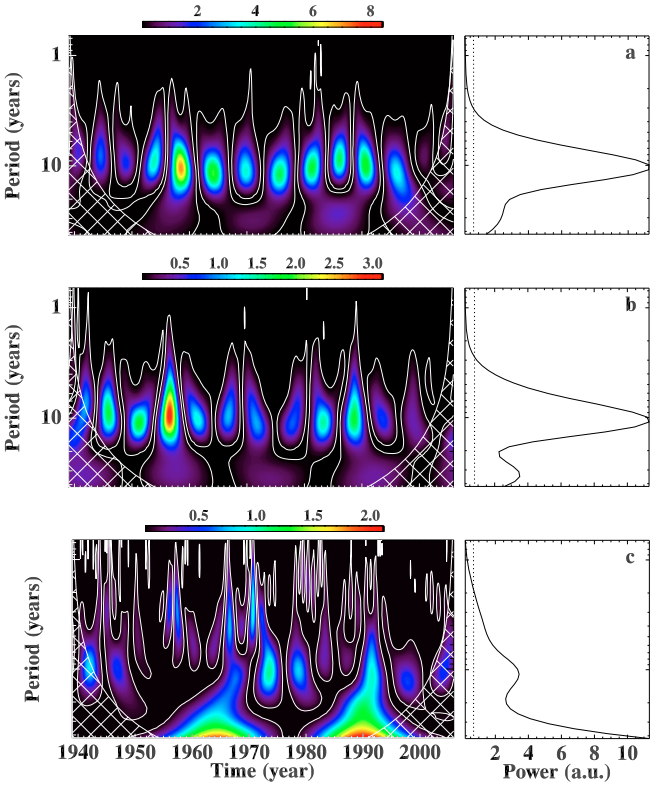

Fig. 8. The most energetic POD modes for the equatorial region. Each panel shows the local wavelet power spectrum $|W_j(T,t)|^2$ of the POD coefficient $a_j(t)$ in the period-time plane (left figure) and the corresponding global wavelet spectrum $P_j(T)$ (right panel). Panels **a), b), c)** refer respectively to $j = 0, 1, 2$. Solid lines in the local and dotted lines in the global spectrum mark the power significance at 95%. Color scale is in arbitrary units.

excess at a period close to 25 years. This low-frequency peak, pronounced in equatorial $j = 1$ and polar $j = 0$ spectra, is reminiscent of the so-called Hale's law (see e.g. Stix 2002), the 22-year cycle related to the inversion of the magnetic field, that could also influence the coronal emissions (Tritakis et al. 1988). The length of our data set, lasting about 45 years, is probably insufficient to precisely detect this period. Although at first sight the coefficient $a_2(t)$ of the equatorial sample does not show any evident periodicity (see Fig. 3, panel c), a peak in the global power spectrum, at about 11 years, can be identified (Fig. 8, panel c). The local wavelet spectrum for the coefficient $j = 2$, although dominated by the 11 year contribution, shows significant power in the low period range typical of the quasi-biennial oscillations. For the polar $j = 1$ coefficients, the signal associated with the quasi-biennial component is the dominant one. This is clearly indicated by the corresponding local spectra where the

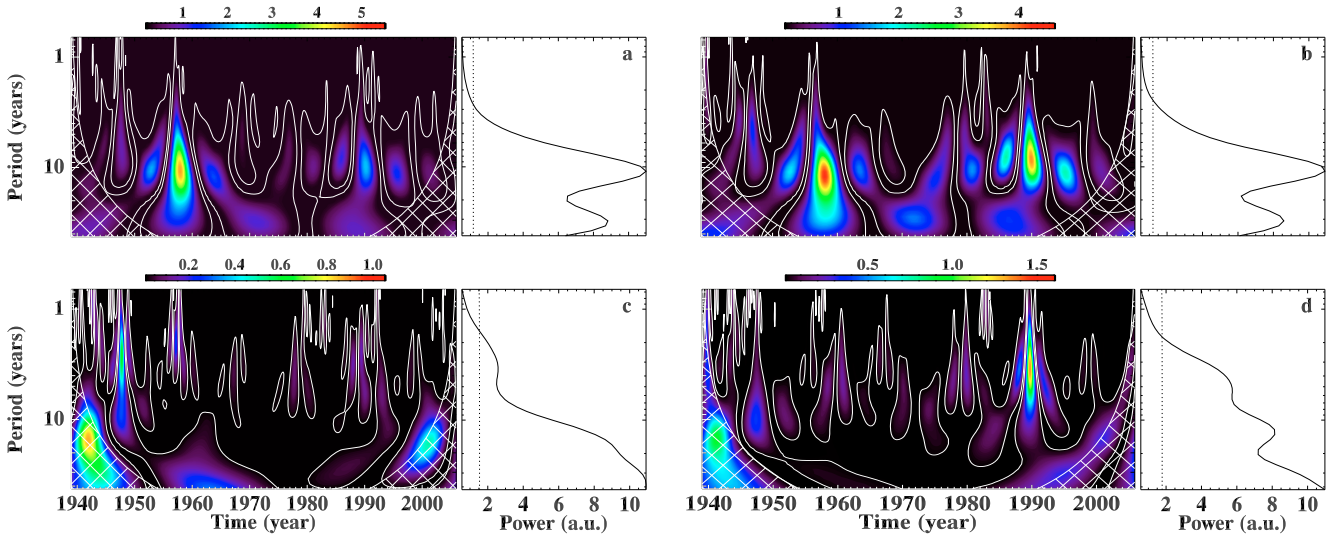

Fig. 9. The most energetic POD modes for the polar regions. Each panel shows the local wavelet power spectrum $|W_j(T,t)|^2$ of the POD coefficient $a_j(t)$ in the period-time plane (*left figure*) and the corresponding global wavelet spectrum $P_j(T)$ (*right figure*). Panels **a)**, **c)** refer respectively to $j = 0, 1$ coefficients of the northern region. Panels **b)**, **d)** refer to $j = 0, 1$ coefficients of the southern region. Solid lines in the local and dotted lines in the global spectrum mark the power significance at 95%. Color scale is in arbitrary units.

highest values of power are distributed at periods shorter than the main 11 years cycle (Fig. 9, panels c, d). The quasi-biennial component of the solar cycle, although weaker than the main one, is very robust since it has been recorded by many indicators (see e.g. Kane 2005; Penza et al. 2006; Li et al. 2006; Cadavid et al. 2005). The peak in $P_j(T)$ corresponding to the short-term contribution, although significant, is underestimated compared to the main cycle peak. This effect is due to the strong modulation or the quasi-biennial frequencies varying from a period to another.

POD, discriminating the different phenomena according to their spatial pattern, is able to separate the main cycle, associated with the classical butterfly pattern, from other components. Moreover the POD modes are orthonormal, so that this analysis in general is able to separate independent phenomena within a complex behaviour. Being captured by the low energy POD modes, the occurrence of the high frequency cycles is a phenomenon energetically less relevant than the main 11-year cycle. The quasi-biennial components, isolated in a single mode by POD, are characterized by similar spatial scales. The quasi-biennial signal is detected, with similar amplitudes, in the analyzed latitude bands: the polar areas, where the contribution to the solar cycle is only due to the large-scale global magnetic field, and the equatorial region, where the cycle is dominated by the emergence of active regions. Our results show that the quasi-biennial periodicity is related to the global large scale magnetic field and its origin must be a phenomenon, within the dynamo process, different from the emergence of active regions (Benevolenskaya 1998; Vecchio & Carbone 2008b) and with turbulent properties, as indicated by the phase-space considerations. In fact it is better detected in the polar regions, while it is masked by the strong and spatially structured 11 year contribution in the equatorial band. However, the strengths of the two mechanisms could be related. As shown by the local wavelet power $|W_j(T,t)|^2$ that furnishes useful information about the time localization of the high-frequency periodicities, the amplitudes of the short-term component are more pronounced during the maxima of the solar main activity.

The joint analysis of POD and wavelet underlines that the period of the detected quasi-biennial high-frequency component is not constant. For the POD coefficients associated with this component, the maximum of the local wavelet power is not fixed but oscillates in time (see Fig. 9, panels c, d). A modulation of the period length, as for the main solar cycle, seems to occur for the quasi-biennial contribution. We can add more harmonics to the "solar melody" generated by the time variation of the period of the main 11-year cycle. The period length variations can be calculated following the approach proposed by Fligge et al. (1999). The method has been applied to measure the period length variations for the quasi-biennial contribution and to recalculate the modulation of the main solar cycle using our dataset rather than the usual sunspot series. The period length at a given time is found by identifying the periods corresponding to local maxima of $|W_j(T,t)|^2$ in a narrow band around $P_0 = 11$ years, for the main component, and $P_1 = 2.5$ years for the quasi-biennial component, and by following them in time. Only the maxima corresponding to a wavelet significance level greater than 95% and outside the COI are taken into account. The error bars assigned to each length represent the wavelet period resolution at the calculated values. The results are presented in Fig. 10 where the time evolution of both periods, of the main and quasi-biennial solar cycle, extracted from the first two POD modes of equatorial, north and south high-latitude samples (panels a–c respectively) is shown. The main 11-year cycle, described by the coefficients $j = 0, 1$ (panel a) of the equatorial and $j = 0$ (panels b, c) of the polar samples, shows the well know modulation with period, oscillating between about 11 and 9.5 years (Friis-Christensen & Lassen 1991; Fligge et al. 1999). The characteristic period of the quasi-biennial component, extracted from coefficients $j = 0$ of the equatorial and $j = 1$ of the polar data sets, varies between 1.5 and 4 years in the range of values in which low-term components of the solar cycle are commonly detected.

4. Discussion and conclusions

The main purpose of this paper is the investigation of the spatio-temporal dynamics of solar activity using time series of the spatial green coronal emission line at 530.3 nm, in the period of time from 1939 to 2005. Besides the main 11-year cycle we

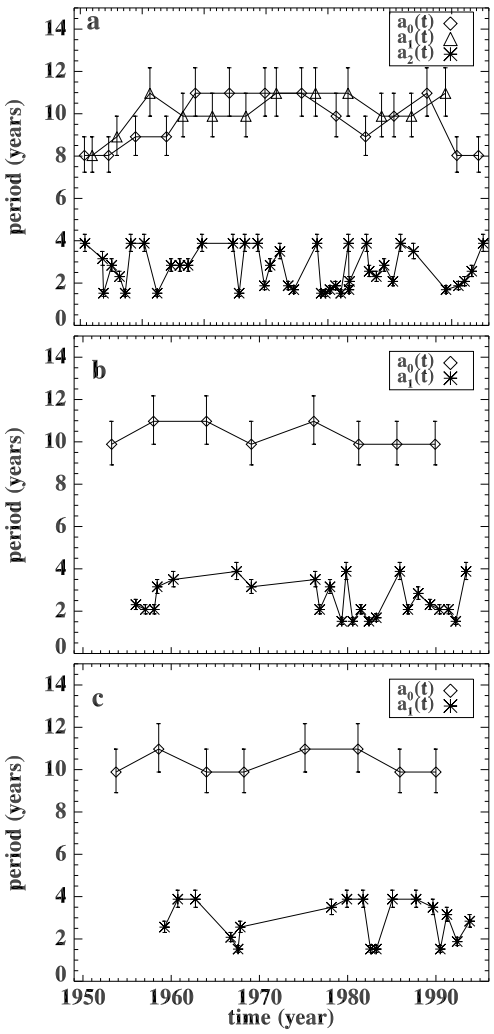

Fig. 10. Time variations of 11 year and quasi-biennial period lengths obtained from the wavelet analysis of the significant POD coefficients for the equatorial region (*upper panel*), the northern region (*middle panel*) and the southern region (*lower panel*).

found a well defined high-frequency quasi-biennial period of activity. The contribution of the 11-year component of the solar activity, being related to the emergence of active regions, is dominant in the equatorial sample, even if it is also present in the polar bands at lower amplitudes. Conversely, the quasi-biennial periodicity is better detected in the polar data, where the contribution to the solar cycle is mainly due to the large scale magnetic field. The energy contents of the two phenomena are noticeably different. This represents a further indication that the high frequency component must be described with a dynamo mechanism different from the process generating the emergence of active regions. This can also be seen by making simple considerations about the phase space, built using two POD coefficients. The phase-space of the modes dominated by 11-year oscillations shows a regular behaviour, explicable as the result of wave-like phenomena. On the other hand, the modes associated with the 2-year component of the solar cycle generate a stochastic pattern. This indicates that the short term component of the solar activity is probably generated by a turbulence-like phenomenon in a narrow band of frequency.

Other properties of the solar cycle can be inferred from our analysis. First of all the high-frequency component shows a variation of the period length over time. Its period changes between 4 years and 1.5 years. We found a good agreement between the frequencies of a quasi-biennial cycle detected by different indicators, observed only in some solar cycles (see e.g. Cadavid et al. 2005; Li et al. 2006; Knaack et al. 2004, 2005), and the calculated lengths in the short-term periods investigated here. All these considerations indicate that this component of the solar activity, commonly considered as a sequence of multiple oscillations with different frequencies, could be simply the manifestation of the temporal modulation of a unique quasi-biennial activity cycle. All the found properties of the cycle represent constraints that should be taken into account in the dynamo models built to describe the source of solar periodicities.

Our analysis of the quasi-biennial solar cycle can be directly related to other astrophysical fields. In particular, the quasi-biennial solar cycle could be correlated to the quasi-biennial variation of solar neutrino fluxes (e.g. Sakurai 1979) and modulate the cosmic ray flux in interplanetary space (Laurenza et al. 2009).

Acknowledgements. We thank the referee for useful comments and help in improving the presentation of results. This work was partially supported by the Italian Space Agency ASI/INAF grant I/015/07/0 "Studi di Esplorazione del Sistema Solare", and by INAF (PRIN-INAF 2007) "Scientific exploitation of the Interferometric Bidimensional Spectrometer (IBIS). Magnetic structuring of the lower solar atmosphere".

References

Badalyan, O. G., Obridko, V. N., & Sýkora, J. 2008, Sol. Phys., 247, 379
Bay, T. 2003, ApJ, 591, 406
Beer, J., Baumgartner, S. T., Dittrich-Hannen, B., et al. 1994, in The Sun as a Variable Star: Solar and Stellar Irradiance Variations (Cambridge: Cambridge Univ. Press), IAU Coll., 143, 291
Benevolenskaya, E. E. 1998, ApJ, 509, L49
Cadavid, A. C., Lawrence, J. K., McDonald, D. P., & Ruzmaikin, A. 2005, Sol. Phys., 226, 359
Eddy, J. A. 1976, Science, 192, 1189
Fligge, M., Solanki, S. K., & Beer, J. 1999, A&A, 346, 313
Friis-Christensen, E., & Lassen, K. 1991, Science, 254, 698
Gnevyshev, M. N. 1977, Sol. Phys., 51, 175
Haubold, H. J. 1998, Astrophys. Space Sci., 258, 201
Holmes, P., Lumley, J. L., & Berkooz, G. 1996, Turbulence, Coherent Structures, Dynamical Systems and Symmetry (Cambridge University Press)
Kane, R. P. 2005, Sol. Phys., 227, 155
Knaack, R., Stenflo, J. O., & Berdyugina, S. V. 2004, A&A, 418, L17
Knaack, R., Stenflo, J. O., & Berdyugina, S. V. 2005, A&A, 438, 1067
Krivova, N. A., & Solanki, S. M. 2002, A&A, 394, 701
Laurenza, M., Storini, M., Giangravé, S., & Moreno, G. 2009, J. Geophys. Res., 114, A01103
Lawrence, J. K., Cadavid, A., & Ruzmaikin, A. 2004, Sol. Phys., 225, 1
Li, K. J., Li, Q. X., Su, T. W., & Gao, P. X. 2006, Sol. Phys., 239, 493
Mininni, P. D., Gómez, D. O., & Mindlin, G. B. 2000, Phys. Rev. Lett., 85, 5476
Mininni, P. D., Gómez, D. O., & Mindlin, G. B. 2002, Phys. Rev. Lett., 89, 061101
Penza, V., Pietropaolo, E., & Livingston, W. 2006, A&A, 454, 349
Pontieri, A., Lepreti, F., Sorriso-Valvo, L., Vecchio, A., & Carbone, V. 2003, Sol. Phys., 213, 195
Rees, D. E., López Ariste, A., Thatcher, J., & Semel, M. 2000, A&A, 355, 759
Rybanský, M., Rusin, V., Minarovjech, M., & Gaspar, P. 1994, Sol. Phys., 152, 153
Rybanský, M., Rušin, V., Minarovjech, M., Klocok, L., & Cliver, E. W. 2005, J. Geophys. Res., 110, A08106
Rušin, V., & Zverko, J. 1990, Sol. Phys., 128, 261
Sakurai, K. 1979, Nature, 278, 146
Sakurai, K., Haubold, H. J., & Shirai, T. 2008, Space Rad., 5, 207
Scafetta, N., & West, B. J. 2008, Physics Today, 61, 50
Shirai, T. 2004, Sol. Phys., 222, 199
Stix, M. 2002, The Sun, an introduction (Berlin: Springer-Verlag)
Torrence, C., & Compo, G. 1998, Bull. Am. Meterol., 79, 61
Tritakis, V. P., Mavromichalaki, H., & Petropoulos, B. 1988, Sol. Phys., 115, 367
Vecchio, A., & Carbone, V. 2008a, Sol. Phys., 249, 11
Vecchio, A., & Carbone, V. 2008b, ApJ, 683, 536
Vecchio, A., Primavera, L., Carbone, V., & Sorriso-Valvo, L. 2005, Sol. Phys., 229, 359
Vecchio, A., Carbone, V., Lepreti, F., et al. 2008, Sol. Phys., 251, 163